Inorganic Chemistry

Article

pubs.acs.org/IC

High-Pressure Synthesis, Crystal Structures, and Properties of $CdMn_7O_{12}$ and $SrMn_7O_{12}$ Perovskites

Yana S. Glazkova,[†,‡] Noriki Terada,[§] Yoshitaka Matsushita,[§] Yoshio Katsuya,[∥] Masahiko Tanaka,[∥] Alexey V. Sobolev,[‡] Igor A. Presniakov,[‡] and Alexei A. Belik*[,†]

[†]International Center for Materials Nanoarchitectonics (WPI-MANA), National Institute for Materials Science (NIMS), Namiki 1-1, Tsukuba, Ibaraki 305-0044, Japan

[‡]Department of Chemistry, Lomonosov Moscow State University, Leninskie Gory, 119992 Moscow, Russia

[§]National Institute for Materials Science (NIMS), Sengen 1-2-1, Tsukuba, Ibaraki 305-0047, Japan

[∥]Synchrotron X-ray Station at SPring-8, NIMS, Kohto 1-1-1, Sayo-cho, Hyogo 679-5148, Japan

Supporting Information

ABSTRACT: We synthesize $CdMn_7O_{12}$ and $SrMn_{7-x}Fe_xO_{12}$ (x = 0, 0.08, and 0.5) perovskites under high pressure (6 GPa) and high temperature (1373−1573 K) conditions and investigate their structural, magnetic, dielectric, and ferroelectric properties. $CdMn_7O_{12}$ and $SrMn_7O_{12}$ are isostructural with $CaMn_7O_{12}$: space group $R\bar{3}$ (No. 148), Z = 3, and lattice parameters a = 10.45508(2) Å and c = 6.33131(1) Å for $CdMn_7O_{12}$ and a = 10.49807(1) Å and c = 6.37985(1) Å for $SrMn_7O_{12}$ at 295 K. There is a structural phase transition at 493 K in $CdMn_7O_{12}$ and at 404 K in $SrMn_7O_{12}$ to a cubic structure (space group $Im\bar{3}$), associated with charge ordering as found by the structural analysis and Mössbauer spectroscopy. $SrMn_{6.5}Fe_{0.5}O_{12}$ crystallizes in space group $Im\bar{3}$ at 295 K with a = 7.40766(2) Å and exhibits spin-glass magnetic properties below 34 K. There are two magnetic transitions in $CdMn_7O_{12}$ with the Néel temperatures T_{N2} = 33 K and T_{N1} = 88 K, and in $SrMn_7O_{12}$ with T_{N2} = 63 K and T_{N1} = 87 K. A field-induced transition is found in $CdMn_7O_{12}$ from about 65 kOe, and T_{N2} = 58 K at 90 kOe. No dielectric anomalies are found at T_{N1} and T_{N2} at 0 Oe in both compound, but $CdMn_7O_{12}$ exhibits small anomalies at T_{N1} and T_{N2} at 90 kOe. In pyroelectric current measurements, we observe large and broad peaks around magnetic phase transition temperatures in $CdMn_7O_{12}$, $SrMn_7O_{12}$, and $SrMn_{6.5}Fe_{0.5}O_{12}$; we assign those peaks to extrinsic effects and compare our results with previously reported results on $CaMn_7O_{12}$. We also discuss general tendencies of the AMn_7O_{12} perovskite family (A = Cd, Ca, Sr, and Pb).

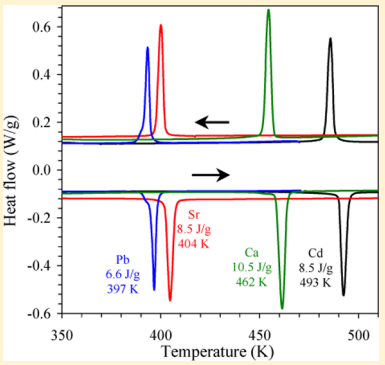

1. INTRODUCTION

$(AA'_3)B_4O_{12}$ perovskite-structure materials have received a lot of attention because many members of this family show interesting physical and chemical properties,[1−3] for example, properties of heavy Fermions,[1] intersite charge transfer and disproportionation,[3,4] metal−insulator transitions, giant dielectric constant,[5] collinear and noncollinear magnetic ordering with high magnetic ordering temperatures,[1] and multiferroic properties.[6] $(AA'_3)B_4O_{12}$ perovskites allow large variations in the chemical composition,[1−10] for example, with A = Na^+, Mn^{2+}, Cd^{2+}, Ca^{2+}, Sr^{2+}, R^{3+} (R = rare earths), and Bi^{3+}; A′ = Cu^{2+}, Mn^{3+}, Co^{2+},[7] and Pd^{2+};[7] and B = $Mn^{3+/4+}$, Fe^{3+}, Cr^{3+}, Al^{3+}, Ti^{4+}, V^{4+}, Ge^{4+}, Sn^{4+}, Ru^{4+}, Ir^{4+}, Ta^{5+}, Nb^{5+}, Sb^{5+}, and others.[1] A very unusual cation order is realized in $(AA'_3)B_4O_{12}$ with 12-fold-coordinated A site and square-coordinated A′ site, the B site has a usual octahedral coordination for perovskites. Because of the highly unusual coordination of the A′ site, this site is typically occupied by Jahn−Teller cations, such as Cu^{2+} and Mn^{3+}, and most of the $(AA'_3)B_4O_{12}$ compounds need high-pressure (HP) and high-temperature (HT) for their preparation.

AMn_7O_{12} perovskites (A = Na, Ca, Cd, Sr, La, and Nd) have been discovered in the 1970s by Marezio et al.[9,10] and intensively investigated because of their complex magnetic and structural transitions.[11−14] This family has recently been extended to A = Bi[15,16] and Pb.[17] Among AMn_7O_{12}, only $CaMn_7O_{12}$ can be prepared at ambient pressure. This is one of the reasons why $CaMn_7O_{12}$ has been investigated a lot.[18−21] The discovery of giant improper ferroelectricity in $CaMn_7O_{12}$ (P = 2870 $\mu C/m^2$)[6] has fuelled additional interest to this family (refs 22−29, just to mention a few).

$CaMn_7O_{12}$ crystallizes in space group $R\bar{3}$ at room temperature.[30] At about 400−450 K, there is a phase transition to a cubic structure (space group $Im\bar{3}$). An incommensurate structural modulation along the hexagonal c axis takes place below about 250 K, associated with orbital ordering (OO).[22] In $CaMn_7O_{12}$, two magnetic transitions occur at T_{N1} = 90 K, to a long-range helical antiferromagnetic (AFM) order with the emergence of giant ferroelectricity of about 2870 $\mu C/m^2$, and at

Received: July 1, 2015
Published: August 31, 2015

DOI: 10.1021/acs.inorgchem.5b01472
Inorg. Chem. 2015, 54, 9081−9091

T_{N2} = 48 K. Structural and physical properties of its analogues, $CdMn_7O_{12}$ and $SrMn_7O_{12}$,[9] have not been investigated yet, probably because they can only be prepared at HP-HT conditions. Only one theoretical work appeared recently about $SrMn_7O_{12}$ predicting a giant electronic polarization.[25] In $PbMn_7O_{12}$, one magnetic transition was found at 68 K without any dielectric anomalies; and no information about ferroelectric polarization was reported.[17]

Therefore, in this work, we describe the HP-HT synthesis, crystal structures, and properties of $CdMn_7O_{12}$ and $SrMn_7O_{12}$. We find two magnetic transitions in $CdMn_7O_{12}$ with the Néel temperatures T_{N2} = 33 K and T_{N1} = 88 K, and in $SrMn_7O_{12}$ with T_{N2} = 63 K and T_{N1} = 87 K, and we observe structural phase transitions at 493 K in $CdMn_7O_{12}$ and at 404 K in $SrMn_7O_{12}$. We also discuss general tendencies of the AMn_7O_{12} perovskites (A = Cd, Ca, Sr, and Pb) and find that T_{N1} is almost constant in all compounds, while T_{N2} rapidly increases with increasing the size of the A cation; the temperature of the $Im\bar{3}$-to-$R\bar{3}$ phase transition associate with charge ordering decreases with increasing the size of the A cation.

2. EXPERIMENTAL DETAILS

$SrMn_{7-x}Fe_xO_{12}$ (x = 0, 0.08, and 0.5) samples were prepared from stoichiometric mixtures of Mn_2O_3, Fe_2O_3 ($^{57}Fe_2O_3$, 95.5% enriched by ^{57}Fe), and 4H-$SrMnO_3$. $CdMn_7O_{12}$ was prepared from a stoichiometric mixture of Mn_2O_3, MnO_2 (99.997%), and CdO (99.99%). The mixtures were placed in Au capsules and treated at 6 GPa in a belt-type high-pressure apparatus at 1573 K for 2 h for $SrMn_{7-x}Fe_xO_{12}$ and at 1373 K for 2 h for $CdMn_7O_{12}$ (heating rate to the desired temperatures was 10 min). After the heat treatments, the samples were quenched to room temperature (RT), and the pressure was slowly released. The samples were black dense pellets. Single-phase Mn_2O_3 was prepared from commercial MnO_2 (99.997%) by heating in air at 923 K for 24 h. Single-phase 4H-$SrMnO_3$ was synthesized from a stoichiometric mixture of Mn_2O_3 and $SrCO_3$ (99.99%) by annealing in air at 1373 K for 48 h and 1273 K for 24 h.[31]

Laboratory X-ray powder diffraction (XRPD) data were collected at RT on a RIGAKU Ultima III diffractometer using CuK$_\alpha$ radiation (2θ range of 10−100°, a step width of 0.02°, and a counting time of 9−12 s/step). Low-temperature XRPD data of $SrMn_7O_{12}$ were measured between 10 and 300 K on a RIGAKU SmartLab instrument using CuKα1 radiation (45 kV, 200 mA; 2θ range of 5−120°, a step width of 0.01°, and scan speed of 4 deg/min) and a cryostat system.

Synchrotron XRPD data were measured between 295 and 580 K on a large Debye−Scherrer camera at the BL15XU beamline of SPring-8.[32,33] The intensity data were collected between 1° and 62° at 0.003° intervals in 2θ; the incident beam was monochromatized at λ = 0.65297 Å. The samples were packed into Lindemann glass capillaries (inner diameter: 0.1 mm), which were rotated during the measurement. The absorption coefficients were also measured, and Rietveld analysis was applied using the RIETAN-2000 program.[34]

Magnetic susceptibilities ($\chi = \mathbf{M}/\mathbf{H}$) were measured using a SQUID magnetometer (Quantum Design, MPMS XL and 1 T) between 2 and 350 K (or 400 K) in different applied magnetic fields under both zero-field-cooled (ZFC) and field-cooled on cooling (FCC) conditions. FCC curves were recorded after ZFC measurements. In a few cases, field-cooled curves on warming (FCW) were measured after FCC measurements. Isothermal magnetization measurements were performed between −70 and 70 kOe at 2 K. Frequency dependent ac susceptibility measurements at different static magnetic fields (H_{dc} = 0, 1, and 10 kOe) were performed with a Quantum Design MPMS-1T instrument from 150 to 2 K at frequencies (f) of 1.99, 110, and 299.5 Hz and applied oscillating magnetic fields (H_{ac}) of 0.05, 0.5, and 5 Oe. Specific heat, C_p, was recorded between 2 and 300 K on cooling and heating at 0−90 kOe by a pulse relaxation method using a commercial calorimeter (Quantum Design PPMS). Dielectric properties were measured using a NOVOCONTROL Alpha-A high performance frequency analyzer between 5 and 300 K in the frequency range of 100 Hz and 2 MHz and different magnetic fields. Pyroelectric current measurements were done with a Keithley 6517B electrometer; temperature and magnetic field were controlled by PPMS. Pieces of pellets were used in magnetic, specific heat, and dielectric measurements. Differential scanning calorimetry (DSC) curves of powder samples were recorded on a Mettler Toledo DSC1 STAR^e system at a heating/cooling rate of 10 K/min between 130 and 873 K for $SrMn_7O_{12}$ and between 130 and 573 K for $CdMn_7O_{12}$ in open Al capsules. Three runs were performed to check the reproducibility, and very good reproducibility was observed.

^{57}Fe Mössbauer spectra were recorded between 77 and 450 K using a conventional constant-acceleration spectrometer. The radiation source ^{57}Co(Rh) was kept at RT. All isomer shifts are referred to α-Fe at 300 K. The experimental spectra were processed and analyzed using methods of spectral simulations implemented in the SpectrRelax program.[35]

3. RESULTS

3.1. Structural Properties of $CdMn_7O_{12}$ and $SrMn_{7-x}Fe_xO_{12}$. $SrMn_7O_{12}$ and $SrMn_{6.92}{}^{57}Fe_{0.08}O_{12}$ contained trace amounts of Mn_2O_3 impurity. $SrMn_{6.5}Fe_{0.5}O_{12}$ contained traces of Mn_2O_3 and 6H-$SrMnO_3$[31] impurities (Figure S1 of Supporting Information). In $CdMn_7O_{12}$, Mn_2O_3 and CdO impurities could be identified, and $CdMn_7O_{12}$ also contained unidentified impurities (Figures S2 and S3). $CdMn_7O_{12}$, $SrMn_7O_{12}$, and $SrMn_{6.92}{}^{57}Fe_{0.08}O_{12}$ crystallize in space group $R\bar{3}$ similar to $CaMn_7O_{12}$[30] and $PbMn_7O_{12}$.[17] Therefore, we used structural parameters of $CaMn_7O_{12}$ as the starting ones in the Rietveld analysis of $CdMn_7O_{12}$ and $SrMn_7O_{12}$. Our refined structural parameters, primary bond lengths, and bond-valence sums (BVS)[36] of $CdMn_7O_{12}$ and $SrMn_7O_{12}$ are summarized in Table 1, and a picture of the crystal structure of $SrMn_7O_{12}$ is shown in Figure 1a. Experimental, calculated, and difference synchrotron XRPD patterns of $SrMn_7O_{12}$ are shown in Figure 2a. Refinements of occupation factors suggested that all sites are fully occupied (Table S1).

$SrMn_{6.5}Fe_{0.5}O_{12}$ at RT and $CdMn_7O_{12}$ and $SrMn_7O_{12}$ at high temperatures (see part 3.2 and Figures S1, S8, and S9) crystallize in the cubic symmetry (space group $Im\bar{3}$); their structural parameters are summarized in Table 2. Figure 1b shows a crystal structure of the cubic phase, and Figure 2b gives synchrotron XRPD patterns of $SrMn_7O_{12}$ at 430 K.

No structural phase transitions were found in $SrMn_7O_{12}$ below RT by laboratory XRPD. However, it could be difficult to detect an incommensurate structural modulation[22] by laboratory XRPD. The a lattice parameter shows no anomalies between 10 and 395 K, while a small anomaly is found near 63 K (= T_{N2}) in the temperature dependence of the c lattice parameter (Figure S4). Controversial temperature dependences of the lattice parameters are given in the literature for $CaMn_7O_{12}$,[1,20,37] with the most reliable data published in ref 37. Our data for $SrMn_7O_{12}$ resemble results for $CaMn_7O_{12}$ from ref 37.

3.2. Structural Phase Transitions in $CdMn_7O_{12}$ and $SrMn_{7-x}Fe_xO_{12}$. The DSC measurements showed the existence of structural phase transitions at T_{str} = 493 K in $CdMn_7O_{12}$, at T_{str} = 404 K in $SrMn_7O_{12}$, and at T_{str} = 379 K in $SrMn_{6.92}{}^{57}Fe_{0.08}O_{12}$ (Figure 3a). T_{str} is noticeably decreased in $SrMn_{7-x}Fe_xO_{12}$, confirming that the iron doping takes place. The enthalpy of the transition is almost the same in $CdMn_7O_{12}$ and $SrMn_7O_{12}$ (8.5 J/g). The transition is much broader in $SrMn_{0.92}{}^{57}Fe_{0.08}O_{12}$, but its enthalpy is close to that of $SrMn_7O_{12}$.

DOI: 10.1021/acs.inorgchem.5b01472
Inorg. Chem. 2015, 54, 9081−9091

Table 1. Structure Parameters, Bond Lengths, and Bond-Valence Sum (BVS) of AMn_7O_{12} (A = Ca and Sr) at Room Temperature

	$CdMn_7O_{12}$	$SrMn_7O_{12}$
a (Å)	10.45508(2)	10.49807(1)
c (Å)	6.33131(1)	6.37985(1)
V (Å^3)	599.348(2)	608.920(1)
B(A) (Å^2)/BVS	1.89(4)/1.66	0.43(3)/2.85
B(Mn1) (Å^2)/BVS	1.30(3)/3.03	0.56(2)/2.88
B(Mn2) (Å^2)/BVS	0.98(3)/3.27	0.32(2)/3.24
B(Mn3) (Å^2)/BVS	1.06(5)/3.80	0.34(4)/3.67
x(O1)	0.2256(5)	0.2244(4)
y(O1)	0.2770(5)	0.2752(4)
z(O1)	0.0820(6)	0.0801(3)
B(O1) (Å^2)	1.60(8)	0.41(4)
x(O2)	0.3402(4)	0.3418(3)
y(O2)	0.5207(4)	0.5205(2)
z(O2)	0.3451(8)	0.3436(7)
B(O2) (Å^2)	1.06(8)	0.10(5)
R_{wp} (%)	5.61	2.69
R_p (%)	3.98	1.92
R_B (%)	3.12	5.00
R_F (%)	4.66	6.33
A–O2 (Å) × 6	2.567(5)	2.597(3)
A–O1 (Å) × 6	2.718(5)	2.712(4)
Mn1–O2 (Å) × 2	1.892(4)	1.906(2)
Mn1–O1 (Å) × 2	1.904(4)	1.929(2)
Mn1–O1 (Å) × 2	2.692(5)	2.715(4)
Mn1–O2 (Å) × 2	2.824(5)	2.823(3)
Mn2–O1 (Å) × 2	1.889(4)	1.894(2)
Mn2–O2 (Å) × 2	2.040(5)	2.039(2)
Mn2–O1 (Å) × 2	2.046(4)	2.053(2)
Mn3–O2 (Å) × 6	1.929(4)	1.942(4)

[a]Space group $R\bar{3}$ (No. 148), Z = 3. A cations (A = Cd and Sr) occupy the 3a site (0, 0, 0); Mn1–9e site (1/2, 0, 0); Mn2–9d site (1/2, 0, 1/2); Mn3–3b site (0, 0, 1/2); O1 and O2–18f site (x, y, z). BVS = $\sum_{i=1}^{N} \nu_i$, $\nu_i = \exp[(R_0 - l_i)/B]$, N is the coordination number, B = 0.37, $R_0(Cd^{2+})$ = 1.904, $R_0(Sr^{2+})$ = 2.118, and $R_0(Mn^{3+})$ = 1.760.[36]

In $CaMn_7O_{12}$, an incommensurate structural modulation is reported near 250 K.[22] We did not observe any DSC anomalies in $SrMn_7O_{12}$ below RT down to 130 K (Figure S5). This fact could indicate the absence of such a transition in $SrMn_7O_{12}$ or could be caused by a very small thermal effect undetectable by our system. However, a very small DSC anomaly was detected in $CdMn_7O_{12}$ near 240 K (Figure S6). To determine its nature and origin, structural studies using high-resolution diffraction data are needed. We obtained indirect support for its intrinsic origin by measuring DSC curves of $CaMn_7O_{12}$, where we observed a similar very weak anomaly near 255 K and a very strong anomaly near 460 K (Figure S7). Temperatures of the DSC anomalies detected in $CaMn_7O_{12}$ are in very good agreement with the reported phase transition temperatures.[6,22,26] Temperature dependence of the unit cell volume in $CdMn_7O_{12}$ and $SrMn_7O_{12}$ is given on Figure 3b (the lattice parameters are given on Figures S8 and S9); the $R\bar{3}$-to-$Im\bar{3}$ structural phase transitions are accompanied by a small increase of the unit cell volume.

3.3. Magnetic Properties of $CdMn_7O_{12}$ and $SrMn_{7-x}Fe_xO_{12}$. Figure 4 gives specific heat data of $CdMn_7O_{12}$ and $SrMn_7O_{12}$ at different magnetic fields. Two magnetic transitions are detected in $CdMn_7O_{12}$ with the Néel

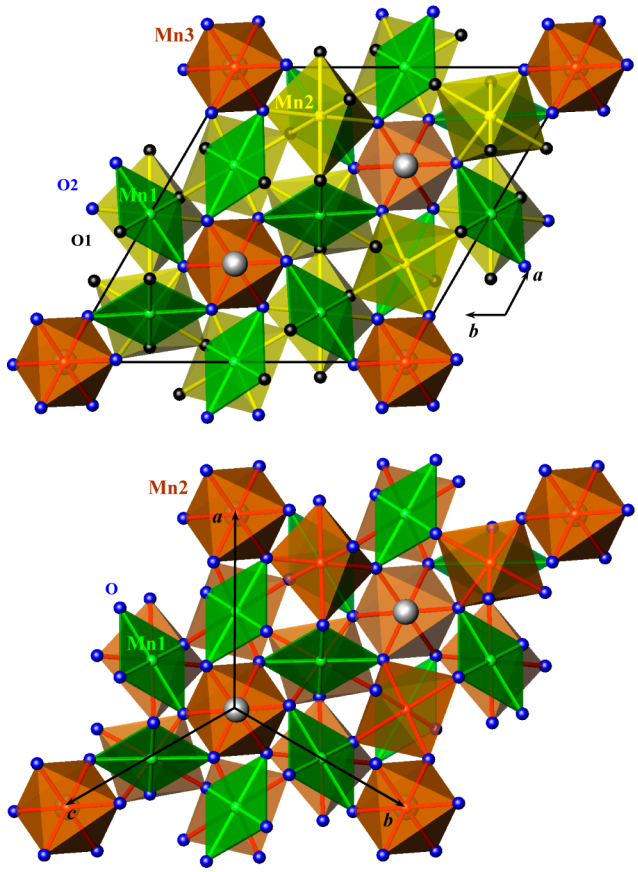

Figure 1. (Top) Projection of the room-temperature crystal structure of $SrMn_7O_{12}$ along the c direction. (Bottom) Projection of the high-temperature cubic crystal structure of $SrMn_7O_{12}$ along the (111) direction. Large gray circles show Sr atoms, and green polyhedra are $Mn1O_4$.

temperatures T_{N2} = 33 K and T_{N1} = 88 K, and in $SrMn_7O_{12}$ with T_{N2} = 63 K and T_{N1} = 87 K. Magnetic fields up to 90 kOe have no effect on the specific heat anomaly at T_{N1} in $CdMn_7O_{12}$ and have a very small effect on the specific heat anomaly at T_{N1} in $SrMn_7O_{12}$. On the other hand, the transitions at T_{N2} are significantly affected by magnetic fields especially in $CdMn_7O_{12}$. The transition at T_{N2} survives up to about 50 kOe in $CdMn_7O_{12}$; above 70 kOe, it is significantly smeared, and a new peak appears at T_{N2}(90 kOe) = 58 K. No temperature hysteresis is found in $SrMn_7O_{12}$ at 0 Oe at T_{N1}, while a tiny hysteresis is observed at T_{N2} (Figure S10); the hysteresis is enhanced in 90 kOe, especially at T_{N2}. Temperature hysteresis is found in $CdMn_7O_{12}$ at 0 Oe (between about 18 and 45 K) and 90 kOe (Figure S11). Because specific heat probes bulk properties, the hysteresis should be intrinsic. The hysteresis behavior near T_{N2} was also observed in $CaMn_7O_{12}$,[29] and we detected hysteresis in the specific heat of $CaMn_7O_{12}$ at T_{N2} (Figure S12). $SrMn_{6.92}{}^{57}Fe_{0.08}O_{12}$ has T_{N2} = 67 K and T_{N1} = 82 K (Figure 4b), while specific heat shows a very weak anomaly near 60 K in $SrMn_{6.5}Fe_{0.5}O_{12}$ (Figure S13). The iron doping has noticeable effects on both T_{N2} and T_{N1}—increasing T_{N2} and decreasing T_{N1} by about 4 K for x = 0.08 in comparison with x = 0 in $SrMn_{7-x}Fe_xO_{12}$.

Magnetic susceptibilities of $CdMn_7O_{12}$ and $SrMn_7O_{12}$ are given on Figure 5. There are very small anomalies at T_{N2} and T_{N1} in both compounds similar to $CaMn_7O_{12}$;[21] the anomalies are more clearly seen at 10 kOe (insets of Figure 5) because a

DOI: 10.1021/acs.inorgchem.5b01472
Inorg. Chem. 2015, 54, 9081–9091

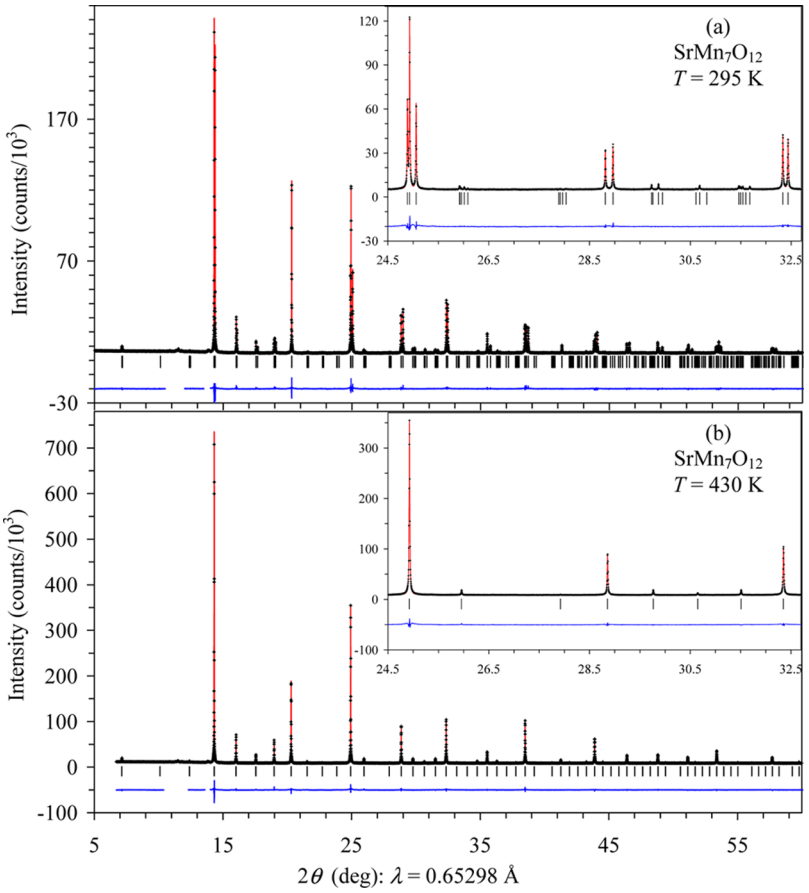

Figure 2. Experimental (black crosses), calculated (red line), and difference (blue line) synchrotron XRPD diffraction patterns of $SrMn_7O_{12}$ at (a) 295 K and (b) 430 K. The bars show possible Bragg reflection positions for $SrMn_7O_{12}$. The insets show enlarged fragments. Missed regions on the difference curves give the excluded regions during the Rietveld refinement.

Table 2. Structure Parameters, Bond Lengths, and Bond-Valence Sum (BVS) of Cubic Modifications of $CdMn_7O_{12}$, $SrMn_7O_{12}$, and $SrMn_{6.5}Fe_{0.5}O_{12}$ at Different Temperatures[a]

	$CdMn_7O_{12}$	$SrMn_7O_{12}$	$SrMn_{6.5}Fe_{0.5}O_{12}$
T (K)	540	430	295
a (Å)	7.37872(2)	7.41238(1)	7.40766(2)
V (Å^3)	401.738(2)	407.261(2)	406.483(2)
B(A) (Å^2)/BVS	2.32(4)/1.66	0.68(2)/2.77	0.71(3)/2.85
B(Mn1) (Å^2)/BVS	1.93(4)/3.00	1.11(2)/2.77	0.94(3)/2.81
B(Mn2) (Å^2)/BVS	1.40(3)/3.33	0.64(2)/3.27	0.47(2)/3.26
y(O)	0.3113(4)	0.3121(2)	0.3116(3)
z(O)	0.1753(5)	0.1772(3)	0.1756(4)
B(O) (Å^2)	2.43(8)	0.78(3)	0.65(4)
R_{wp}	6.00	2.84	3.62
R_p	4.30	1.94	2.42
R_B	4.72	3.50	3.70
R_F	5.09	4.82	4.06
A–O (Å) × 12	2.636(3)	2.661(2)	2.650(3)
Mn1–O (Å) × 4	1.900(3)	1.915(2)	1.907(2)
Mn1–O (Å) × 4	2.771(3)	2.768(2)	2.779(3)
Mn2–O (Å) × 6	1.978(1)	1.984(1)	1.986(1)

[a]Space group $Im\bar{3}$ (No. 204), Z = 2. A cations (A = Cd and Sr) occupy the 2*a* site (0, 0, 0); Mn1–6*b* site (0, 1/2, 1/2); Mn2–8*c* site (1/4, 1/4, 1/4); O – 24*g* site (0, *y*, *z*).

weak ferromagnetic moment, which is developed below T_{N2}, is suppressed by magnetic fields. The inverse FCC magnetic susceptibilities (at 100 Oe) between 200 and 390 K are fit by the Curie–Weiss equation

$$\chi(T) = \mu_{eff}^2 N(3k_B(T-\theta))^{-1} \quad (1)$$

where μ_{eff} is the effective magnetic moment, N is Avogadro's number, k_B is Boltzmann's constant, and θ is the Weiss constant. We obtain values of μ_{eff} = 12.751(16)μ_B and θ = −59.9(9) K for $CdMn_7O_{12}$ and μ_{eff} = 12.829(11)μ_B and θ = −6.4(5) K for $SrMn_7O_{12}$ (Figures 6 and S14; Table 3) close to the expected value of 12.61μ_B for six Mn^{3+} ions and one Mn^{4+} ion. The FCC and FCW curves of $CdMn_7O_{12}$ exhibit a noticeable hysteresis (the inset of Figure 5a and Figure S15), while a very small hysteresis is found in $SrMn_7O_{12}$ between the FCC and FCW curves (Figure S16). It is interesting that ZFC and FCW curves of $CdMn_7O_{12}$ show an additional anomaly near 50 K at 0.1 and 10 kOe (Figure S15). The χ vs T curves of $SrMn_{6.92}{}^{57}Fe_{0.08}O_{12}$ are similar to those of $SrMn_7O_{12}$, but with a weaker ferromagnetic-like response below T_{N2} (Figure S18). The χ vs T curves of $SrMn_{6.5}Fe_{0.5}O_{12}$ exhibit divergence between ZFC and FCC curves at 34 K typical for spin-glass transitions (Figure S19).[23] However, *ac* susceptibility measurements show a very small frequency dependence between 2 and 500 Hz (Figure S20).

Isothermal magnetization data of $SrMn_{7-x}Fe_xO_{12}$ (x = 0, 0.08, and 0.5) and $CdMn_7O_{12}$ at 2 K are given in Figure 7. There is a weak hysteresis in $SrMn_{7-x}Fe_xO_{12}$ (x = 0, 0.08, and 0.5) in agreement with the appearance of weak ferromagnetic response on the χ vs T curves. The M vs H curves of

DOI: 10.1021/acs.inorgchem.5b01472
Inorg. Chem. 2015, 54, 9081–9091

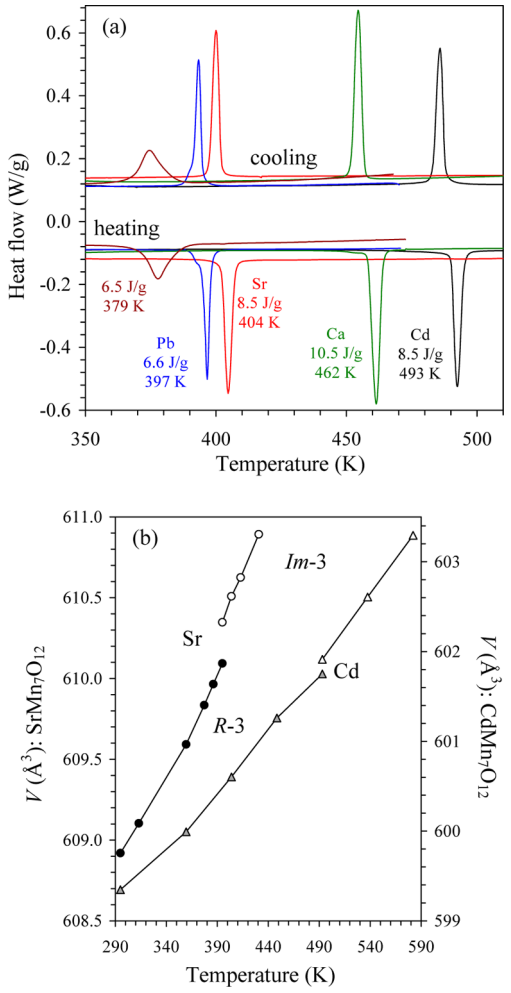

Figure 3. (a) Fragments of differential scanning calorimetry curves of $CdMn_7O_{12}$ (black), $CaMn_7O_{12}$ (green), $SrMn_7O_{12}$ (red), $PbMn_7O_{12}$ (blue), and $SrMn_{6.92}{}^{57}Fe_{0.08}O_{12}$ (brown) on heating and cooling (10 K/min). Second runs (among three runs) are shown. Numbers show peak positions (in K) and peak areas (in J/g) (on heating). (b) Temperature dependence of the unit cell volume (V for the $R\bar{3}$ phase and 1.5V for the $Im\bar{3}$ phase) in $CdMn_7O_{12}$ (triangles) and $SrMn_7O_{12}$ (circles).

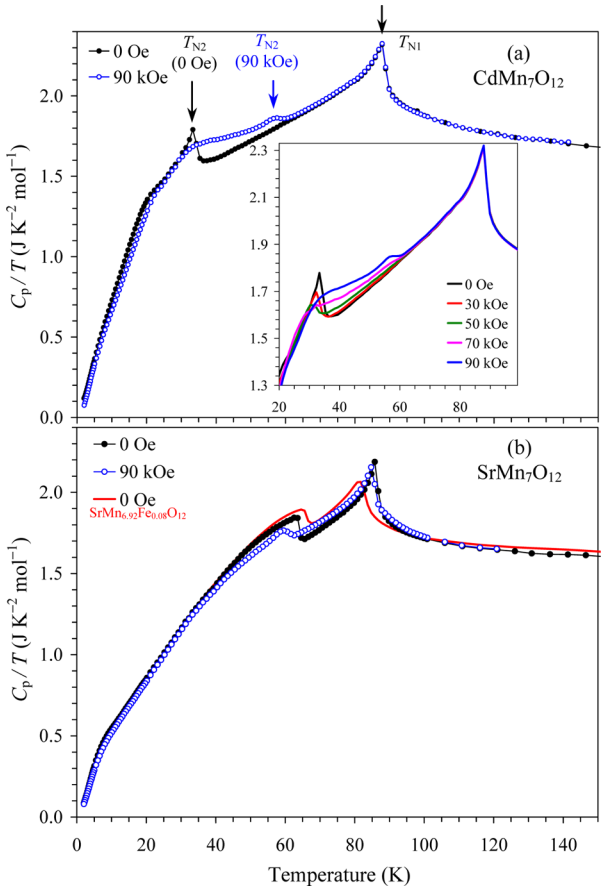

Figure 4. Specific heat data of (a) $CdMn_7O_{12}$ and (b) $SrMn_7O_{12}$ at a zero magnetic field (black filled circles) and 90 kOe (blue empty circles) plotted as C_p/T vs T. The inset in (a) gives fragments of the C_p/T vs T curves of $CdMn_7O_{12}$ at 0, 30, 50, 70, and 90 kOe; arrows show the Néel temperatures. The C_p/T vs T curve of $SrMn_{6.92}{}^{57}Fe_{0.08}O_{12}$ at 0 Oe (red line) is also given on (b). All the curves are measured on cooling.

$CdMn_7O_{12}$ show the existence of a field-induced transition at about 65 kOe in agreement with the specific heat data. The M vs H curves of $SrMn_{6.5}Fe_{0.5}O_{12}$ are typical for spin-glasses (Figure S21).[23]

Figure 8 depicts *ac* susceptibilities of $SrMn_7O_{12}$. Weak frequency-independent anomalies are seen at T_{N2} and T_{N1}. Below T_{N2}, additional frequency-dependent anomalies appear on the χ'' vs T curves. *ac* susceptibilities of $SrMn_7O_{12}$ are independent of H_{ac} (Figure S22), but they significantly depend on H_{dc} (Figure S23). *ac* susceptibilities of $CdMn_7O_{12}$ are basically featureless without clear anomalies at T_{N2} and T_{N1} (Figure S24).

3.4. Mössbauer Spectroscopy of $SrMn_{6.92}{}^{57}Fe_{0.08}O_{12}$ and $SrMn_{6.5}Fe_{0.5}O_{12}$. Figure 9a gives a typical ^{57}Fe Mössbauer spectrum of $SrMn_{6.92}{}^{57}Fe_{0.08}O_{12}$ in the paramagnetic temperature range ($T > T_{N1}$) and below the structural phase transition ($T < T_{str}$). All spectra in this temperature range can be represented as a superposition of two quadrupole doublets (Fe1 and Fe2) with nearly the same isomer shifts (δ) and significantly different quadrupole splittings (Δ), thus indicating that ^{57}Fe probe atoms are located in two nonequivalent crystallographic sites. The best-fit hyperfine parameters of the partial spectra are given in Table 4. Upon heating well above T_{str}, the Mössbauer spectrum (Figure 9b) shows an abrupt convergence of two quadrupole doublets, observed in the $R\bar{3}$ phase, into one quadrupole doublet in the cubic phase. In the low-temperature range (77 K < T < T_{N1}), the spectra show a diffuse resonance absorption peak (Figure 10a), suggesting the existence of a continuous distribution of hyperfine magnetic fields (H_{hf}) at ^{57}Fe nuclei. To analyze such nonresolved spectra, we reconstruct hyperfine field distributions $p(H_{hf})$ (the inset in Figure 10a). From the temperature dependence of the mean field $<H_{hf}>$ and dispersion $D_{p(H)}$ of the resulting distributions $p(H_{hf})$ (Figure 10b), we determine the Néel temperature, which is 79(1) K based on the Mössbauer spectroscopy results. Mössbauer spectrum of $SrMn_{6.5}Fe_{0.5}O_{12}$ is shown on Figure 9c, and its parameters are given in Table 4.

3.5. Pyroelectric Current Measurements and Dielectric Constants of $CdMn_7O_{12}$ and $SrMn_7O_{12}$. In order to check the appearance of ferroelectric polarization in $CdMn_7O_{12}$, $SrMn_7O_{12}$, and $SrMn_{6.5}Fe_{0.5}O_{12}$, we measured electric currents with a standard pyroelectric current procedure. After applying an electric field at 100 K above T_{N1}, we cooled a sample below the Néel temperature, turned the field off, and then measured electric current with warming. It should be

DOI: 10.1021/acs.inorgchem.5b01472
Inorg. Chem. 2015, 54, 9081−9091

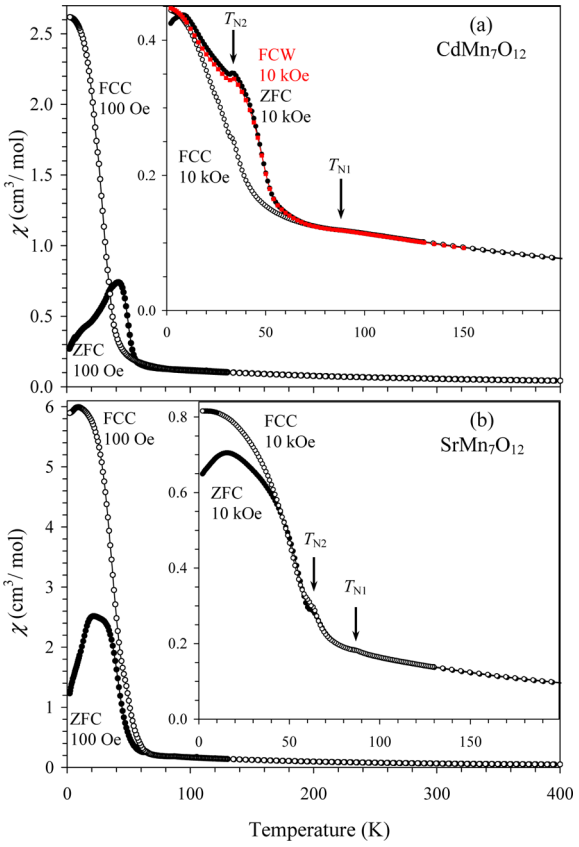

Figure 5. ZFC (black circles) and FCC (white circles) *dc* magnetic susceptibility ($\chi = M/H$) curves of (a) $CdMn_7O_{12}$ and (b) $SrMn_7O_{12}$ at 100 Oe and 10 kOe (the insets). Arrows show the Néel temperatures. For $CdMn_7O_{12}$, the FCW curve at 10 kOe (red squares) is also shown in the inset.

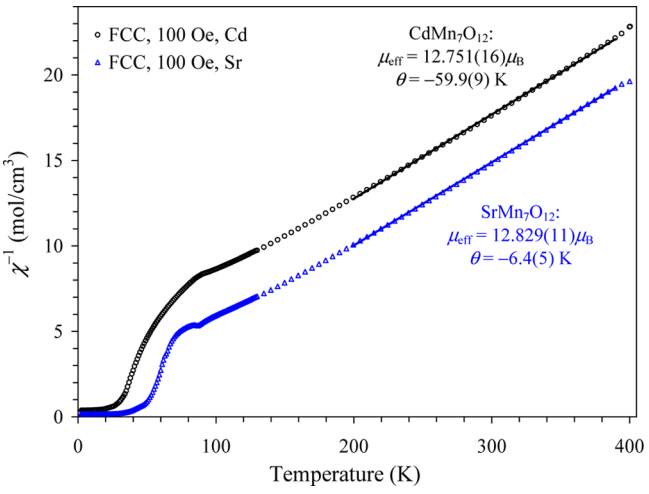

Figure 6. Inverse FCC curves (χ^{-1} vs T) of $CdMn_7O_{12}$ and $SrMn_7O_{12}$ measured at 100 Oe (symbols). The parameters (μ_{eff} and θ) of the Curie–Weiss fits (lines) between 200 and 390 K are given.

noted that electric resistivity in all the samples at 100 K was not "infinite" (with our system), but ~10 GΩ for $CdMn_7O_{12}$ and $SrMn_7O_{12}$, and ~10 MΩ for $SrMn_{6.5}O_{0.5}O_{12}$. Figure 11 shows the results obtained in the above procedure. In $CdMn_7O_{12}$ and $SrMn_7O_{12}$, very large and broad peaks were observed around 90 K, which is near T_{N1} (= 88 and 87 K, respectively). In $SrMn_{6.5}Fe_{0.5}O_{12}$, on the other hand, one negative and one positive peaks appear at 53 and 62 K, respectively. The former does not coincide with any magnetic phase transitions (34 and 60 K seen in Figures S19 and S13), though the latter is near the anomaly observed on specific heat. In $CdMn_7O_{12}$ and $SrMn_7O_{12}$, we observed small negative peaks around 80 K similar to $SrMn_{6.5}Fe_{0.5}O_{12}$, which do not coincide with any magnetic phase transitions.

As shown in Figure 11, we could tune and reverse the electric current value by changing the sign of the poling electric field in $CdMn_7O_{12}$ and $SrMn_7O_{12}$. Absolute values of the current are almost proportional to temperature sweeping rate (Figure S25). These features resemble an intrinsic pyroelectric current. However, we could not conclude that the observed currents are pyroelectric ones by the following reasons. (i) All the temperatures at which peaks appear in electric current do not coincide with the phase transition temperatures observed in the other measurements. (ii) The peaks observed in all the samples are significantly broad, in spite of sharp phase transitions observed at T_{N1} in the other measurements, and the peaks are symmetrical near the maximum. (iii) The electric resistivity around 100 K and near the temperature where a broad peak appears is not "infinite" (by our system). (iv) We observed a similar current in $SrMn_{6.5}Fe_{0.5}O_{12}$ (Figure 11c), which exhibits spin-glass magnetic properties. Therefore, we suggest that the broad peaks in electric current in these samples can be caused by thermally stimulated current (TSC) that is generally observed in semiconductors.[38] For further understanding the phenomena, detailed electric resistivity and TSC measurements on different samples are needed.

We also measured the dielectric constants in $CdMn_7O_{12}$, $SrMn_7O_{12}$, and $SrMn_{6.5}Fe_{0.5}O_{12}$ (Figures 12 and S26–S34). In $CdMn_7O_{12}$, we did not find any anomalies at T_{N1} and $H = 0$ Oe, while a step like anomaly was found in $H \geq 30$ kOe. This result indicates that the phase transition at T_{N1} gets clearer with increasing a magnetic field. A broad dielectric peak was observed in $CdMn_7O_{12}$ near T_{N2} (= 58 K) above about 70 kOe. The dielectric constant shows quite a large value especially for $H = 0$ Oe even below T_{N2}. It infers that local electric dipole moments are strongly fluctuating even at low temperature. Temperature hysteresis is detected between about 15 and 45 K (at 0 Oe) and 15 and 65 K (at 90 kOe) on dielectric constant of $CdMn_7O_{12}$ in agreement with the specific heat and magnetic measurements. $CdMn_7O_{12}$ exhibits a magnetodielectric effect up to 13% at 20 K and 90 kOe (Figure 12b). In $SrMn_7O_{12}$, we did not see any dielectric anomalies at the magnetic phase transition temperatures between 0 and 90 kOe (Figures S26–S29), and a magnetodielectric effect was very small (Figure S35).

4. DISCUSSION

All AMn_7O_{12} with A^{2+} = Cd, Ca, Sr, and Pb crystallize in space group $R\bar{3}$ at RT in comparison with monoclinic RMn_7O_{12} with R = La, Pr, and Bi and $NaMn_7O_{12}$. All AMn_7O_{12} show a structural phase transition from $R\bar{3}$ to $Im\bar{3}$ at high temperatures. The phase transition temperature decreases with increasing the size of A^{2+} cation (Table 3) from 493 K for $CdMn_7O_{12}$ to 397 K for $PbMn_7O_{12}$. One can expect that $BaMn_7O_{12}$ should be cubic at RT. Our attempts to synthesize $BaMn_7O_{12}$ at 6 GPa were not successful; no perovskite phases were formed. It is possible that much higher pressure is needed for the preparation of $BaMn_7O_{12}$ similar to $BaOsO_3$ perovskite (prepared at 17 GPa).[39] From the other side of the AMn_7O_{12} family, $MnMn_7O_{12}$ was reported with triclinic symmetry and

DOI: 10.1021/acs.inorgchem.5b01472
Inorg. Chem. 2015, 54, 9081–9091

Table 3. Phase Transition Temperatures and Parameters of the Curie–Weiss Fits of AMn_7O_{12} with A^{2+} = Cd, Ca, Sr, and Pb[a]

cation	radius, r_{XII} (Å)	T_{str} (K) ≡ T_{CO}	T_{OO} (K)	T_{N2} (K)	T_{N1} (K)	μ_{eff} (μ_B/f.u.)	θ (K)
Cd^{2+}	1.31	493	240	33	88	12.751(16)	−59.9(9)
Ca^{2+}	1.34	462	255	48	91	12.85(4)	−18(2)
Sr^{2+}	1.44	404	?	63	87	12.829(11)	−6.4(5)
Pb^{2+}	1.49	397	?	78	82	12.843(8)	−25.6(4)

[a]Our results are used for all compounds. The Curie–Weiss fits are performed between 200 and 390 K for the FCC data at 100 Oe. T_{CO}: charge-ordering temperature, T_{OO}: orbital-ordering temperature, T_N: Néel temperature. f.u.: formula unit.

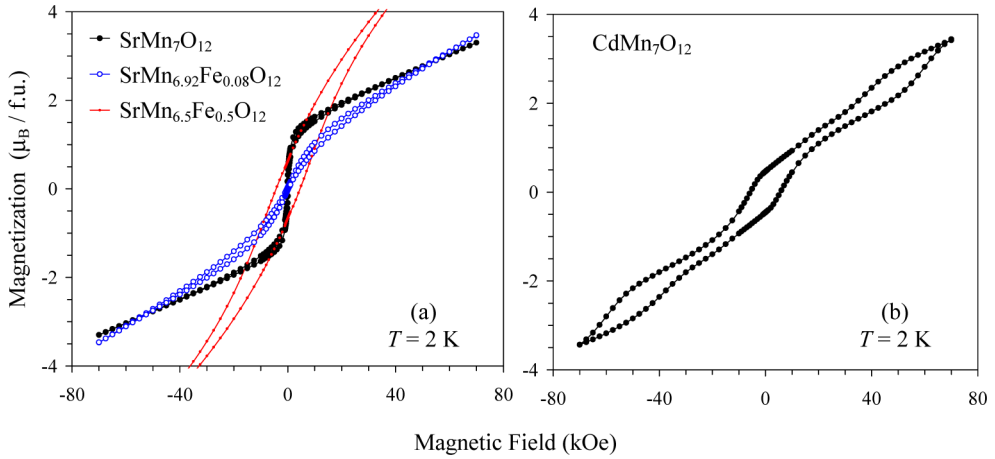

Figure 7. (a) M vs H curves of $SrMn_7O_{12}$, $SrMn_{6.92}{}^{57}Fe_{0.08}O_{12}$, and $SrMn_{6.5}Fe_{0.5}O_{12}$ at 2 K. (b) M vs H curves of $CdMn_7O_{12}$ at 2 K. f.u.: formula unit.

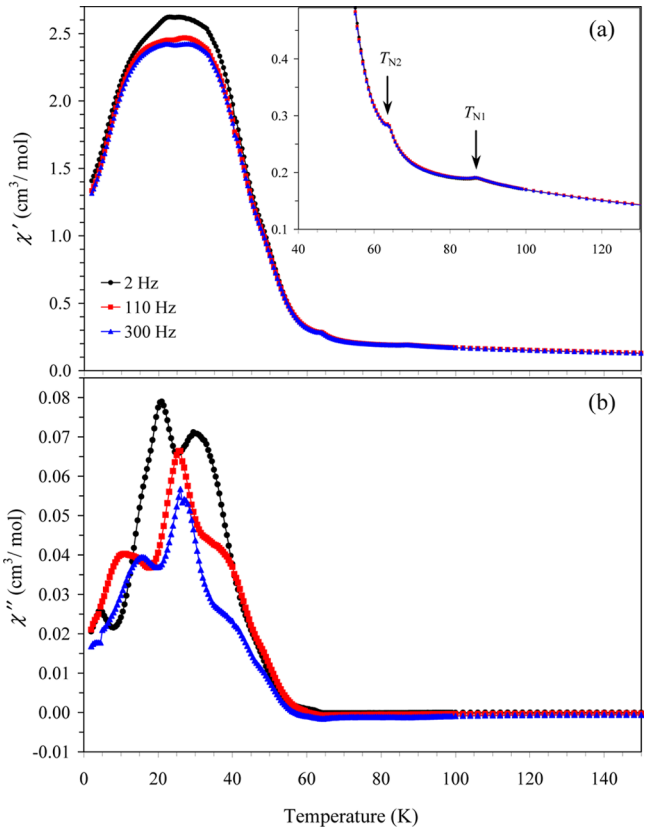

Figure 8. (a) Real parts of the *ac* susceptibility (χ' vs T) and (b) imaginary parts of the *ac* susceptibility (χ'' vs T) for $SrMn_7O_{12}$. Measurements were performed on cooling from 150 to 2 K at a zero static magnetic field using an *ac* field with the amplitude H_{ac} = 5 Oe and frequencies f = 2, 110, and 300 Hz. The inset in (a) shows details near T_{N2} and T_{N1}.

magnetic anomalies at T_{N1} = 99 K, T_{N2} = 47 K, and T_{N3} = 12 K;[40] the symmetry lowering could be caused by a very small size of Mn^{2+} ions (the ionic radius, r_{VIII} = 0.96 Å)[41] or by small oxygen nonstoichiometry. $MnMn_7O_{12}$ requires about 18–22 GPa for the preparation. Other divalent cations, such as, Mg^{2+}, Zn^{2+}, and Fe^{2+}, are even smaller than Mn^{2+}, and the synthesis of AMn_7O_{12} with them would require much higher pressure.

The $Im\bar{3}$-to-$R\bar{3}$ structural phase transition in AMn_7O_{12} is associated with charge ordering of Mn^{3+} and Mn^{4+} cations in the B sublattice.[30] The BVS values for the Mn1 sites in the $Im\bar{3}$ and $R\bar{3}$ phases are close to +3 (Tables 1 and 2) indicating that the A′ site is always occupied by Mn^{3+} cations. In the $Im\bar{3}$ phase, there is one regular $Mn2O_6$ octahedron with six equivalent Mn–O bond lengths of 1.98–1.99 Å and a BVS value of about +3.3 (the average oxidation state of manganese at the B site is +3.25). In the $R\bar{3}$ phase, there is one regular $Mn3O_6$ octahedron with six equivalent Mn–O bond lengths of 1.93–1.94 Å and the BVS value of +3.7–3.8, and there are Mn_2O_6 octahedra with a strong Jahn–Teller distortion and the BVS value of +3.2–3.3. Note that the $Mn2O_6$ octahedron is an apically contracted octahedron in comparison with usually observed apically alongated octahedra.[30] Mössbauer spectroscopy supports the charge-ordering scenario in $SrMn_7O_{12}$ below T_{str}, without any additional transitions down to T_{N1}. Mössbauer spectra of $SrMn_{6.92}Fe_{0.08}O_{12}$ at all temperatures are close to those of $CaMn_{6.97}Fe_{0.03}O_{12}$.[42] The isomer shifts of the Fe1 and Fe2 doublets correspond to high-spin Fe^{3+} ions located in sites with octahedral oxygen coordination. On the basis of the quadrupole splittings values ($\Delta_{Fe1} \gg \Delta_{Fe2}$), the Fe1 doublet should arise from Fe^{3+} cations located at the Mn2 site exhibiting a strong Jahn–Teller distortion from Mn^{3+} ions ($t_{2g}{}^3e_g{}^1$), and the Fe2 doublet should originate from Fe^{3+} cations located at the Mn3 site having Mn^{4+} ions ($t_{2g}{}^3$) with symmetric oxygen surrounding. One doublet is observed above T_{str} with a very small quadrupole splitting, suggesting almost symmetrical

DOI: 10.1021/acs.inorgchem.5b01472
Inorg. Chem. 2015, 54, 9081–9091

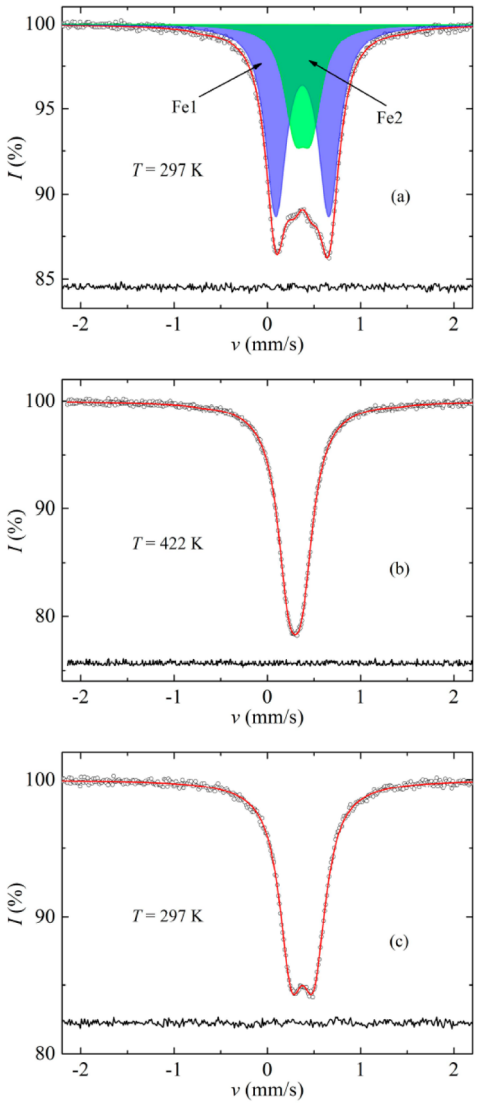

Figure 9. ^{57}Fe Mössbauer spectra of $SrMn_{6.92}{}^{57}Fe_{0.08}O_{12}$ at (a) 297 K and (b) 422 K and (c) Mössbauer spectrum of $SrMn_{6.5}Fe_{0.5}O_{12}$ (20% ^{57}Fe) at 297 K (circles). The solid red lines are the simulation of the experimental spectra as described in the text; parameters of the fits are given in Table 4. The line at the bottom shows the difference between the experimental and calculated curves.

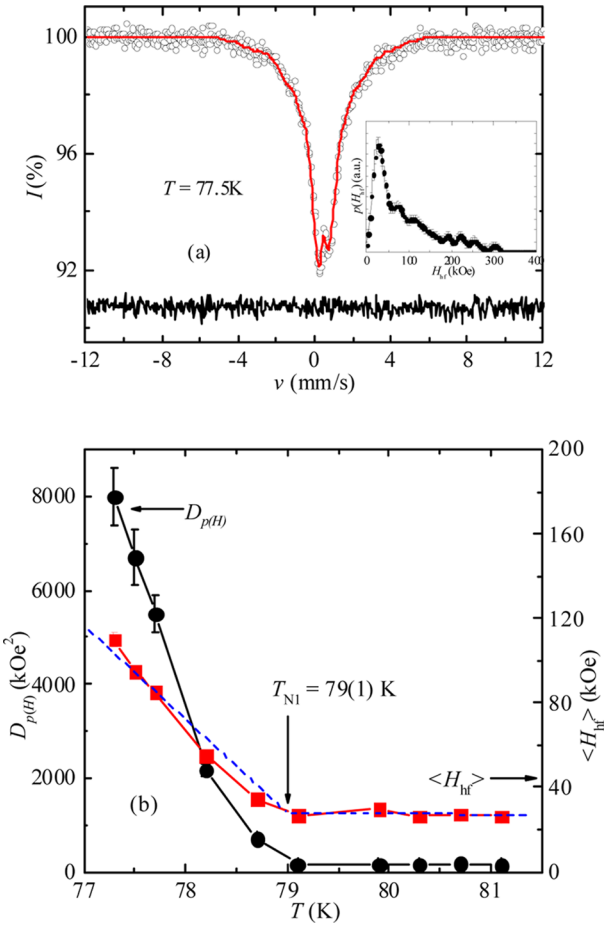

Figure 10. (a) ^{57}Fe Mössbauer spectrum of $SrMn_{6.92}{}^{57}Fe_{0.08}O_{12}$ at 77.5 K. The inset shows the hyperfine field distribution $p(H_{hf})$. (b) Temperature dependence of the average value of the hyperfine field <H_{hf}> (squares) and dispersion $D_{p(H)}$ (circles) of the distributions $p(H_{hf})$.

oxygen surrounding; its isomer shift is reduced because of high temperature. At RT, isomer shifts of $SrMn_{6.92}Fe_{0.08}O_{12}$ and cubic $SrMn_{6.5}Fe_{0.5}O_{12}$ are the same. Note that the experimental intensity ratio of the Fe1 and Fe2 doublets (2:1) is different from the expected one (3:1) from the structure. The same tendency was found in $CaMn_{6.97}Fe_{0.03}O_{12}$;[42] this fact needs further understanding.

The A−O bond lengths in AMn_7O_{12} with A^{2+} = Cd, Ca, and Sr are almost the same: l(Cd−O) = 2.567 and 2.718 Å, l(Ca−O) = 2.588 and 2.678 Å,[30] and l(Sr−O) = 2.597 and 2.712 Å. These bond lengths result in the following BVS values: + 1.66 for Cd^{2+}, + 2.00 for Ca^{2+}, and +2.85 for Sr^{2+}. Therefore, the size of Ca^{2+} almost perfectly matches with the size of the cavity created by the framework of the MnO_6 and MnO_{4+4} polyhedra. This fact could be a reason why only $CaMn_7O_{12}$ can be synthesized at ambient pressure. Cd^{2+} ions are highly underbonded in $CdMn_7O_{12}$ in such a cavity, while Sr^{2+} ions are highly overbonded in $SrMn_7O_{12}$. This is why they can be stabilized only at high pressure, where pressure seems to stabilize the framework with quite different fillings of the cavity.

Table 4. Hyperfine Parameters of ^{57}Fe Mössbauer Spectra of $SrMn_{6.92}{}^{57}Fe_{0.08}O_{12}$ and $SrMn_{6.5}Fe_{0.5}O_{12}$ (20% of ^{57}Fe)[a]

temperature (K)	sample	sites	δ (mm/s)	Δ (mm/s)	W (mm/s)	I (%)
297	$Fe_{0.08}$	Fe1	0.37(1)	0.57(1)	0.28(1)	66.8(2)
	$Fe_{0.08}$	Fe2	0.38(1)	0.18(1)	0.28(1)[b]	33.2(2)
422	$Fe_{0.08}$	Fe	0.30(1)	0.14(1)	0.30(1)	100
297	$Fe_{0.5}$	Fe	0.38(1)	0.25(1)	0.32(1)	100

[a] δ is an isomer shift, Δ is quadrupole splitting, W is line width, and I is a relative intensity. [b] W parameters were constrained to be the same for the Fe1 and Fe2 sites.

DOI: 10.1021/acs.inorgchem.5b01472
Inorg. Chem. 2015, 54, 9081−9091

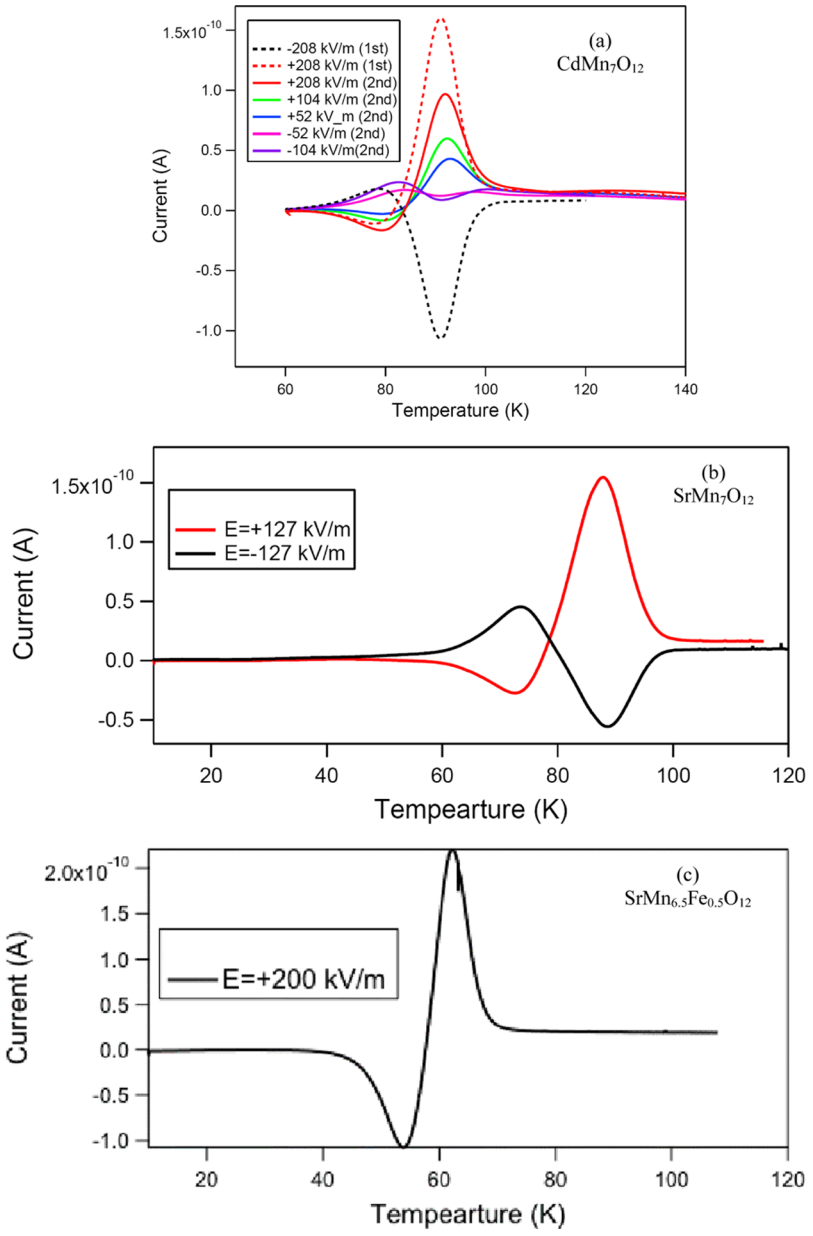

Figure 11. (a) Results of pyroelectric current measurements for $CdMn_7O_{12}$. The dotted lines denote results of the first experiment, while the solid lines represent results of the second experiment. (b) Results of pyroelectric current measurements for $SrMn_7O_{12}$. (c) Results of pyroelectric current measurements for $SrMn_{6.5}Fe_{0.5}O_{12}$.

Under-bonding of Cd^{2+} could explain its relatively large thermal parameter B (Table 1).

T_{N1} is almost the same for AMn_7O_{12} with A^{2+} = Cd, Ca, Sr, and Pb (Table 3), while T_{N2} increases with increasing the radius of the A cation and approaches T_{N1} in $PbMn_7O_{12}$. Therefore, the first magnetic transition is quite rigid and should be determined by the framework of the MnO_6 and MnO_{4+4} polyhedra (Figure 1). On the other hand, the second magnetic transition should be determined by a tiny balance of the A−O bond covalency and Mn−O−Mn bond angles. It is interesting that T_{N3} = 12 K was assumed in $MnMn_7O_{12}$ from the kink on the C_p/T vs T curve;[40] we see the similar kinks at about 21 K in $CdMn_7O_{12}$ and about 8 K in $SrMn_7O_{12}$ (Figure 4). Dielectric data of $CdMn_7O_{12}$ and $SrMn_7O_{12}$ show very broad anomalies at the same temperatures, 21 K in $CdMn_7O_{12}$ (Figures 12 and S30) and 8 K in $SrMn_7O_{12}$ (Figures S28 and S29). But neutron diffraction data of $CaMn_7O_{12}$ showed no further transitions in addition to T_{N1} = 91 K and T_{N2} = 48 K.[6] We note that dielectric anomalies near 21 K at 0 Oe and near 58 K at 90 kOe in $CdMn_7O_{12}$ are too broad to be associated with true ferroelectric transitions.

In our pyroelectric current measurements, we observe large, broad, and symmetrical peaks in all the samples. As mentioned above, these peaks might not be caused by intrinsic pyroelectric current but TSC. We should compare here these data with previously reported data for the related compound $CaMn_7O_{12}$.[21,29] Zhang et al.[21] and Sannigrahi et al.[29] have reported pyroelectric current measurements on polycrystalline $CaMn_7O_{12}$ samples. They also observed broad symmetrical peaks (corresponding to the reported large ferroelectric polarization of 240 $\mu C/m^2$ and 440 $\mu C/m^2$, respectively) at ~70 K and ~60 K, respectively, which do not coincide with T_{N1}

DOI: 10.1021/acs.inorgchem.5b01472
Inorg. Chem. 2015, 54, 9081−9091

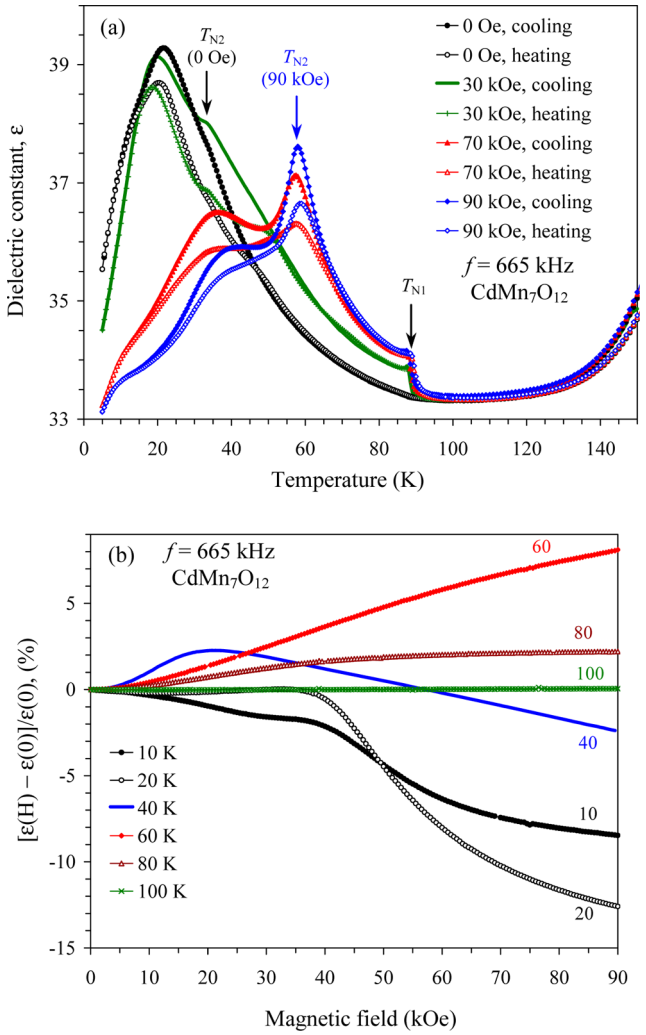

Figure 12. (a) Temperature dependence of dielectric constant of $CdMn_7O_{12}$ at various magnetic fields on cooling and heating at one frequency f = 665 kHz. The vertical arrows mark the Néel temperatures (T_N). (b) The magnetic field dependence of magnetodielectric ratio, $\varepsilon_{MD} = [\varepsilon(H) - \varepsilon(0)]/\varepsilon(0) \times 100]$, of $CdMn_7O_{12}$ at various temperatures and fixed f = 665 kHz.

of 91 K. These features are similar to our present results on $CdMn_7O_{12}$ and $SrMn_7O_{12}$. If we integrate the measured electric current in $CdMn_7O_{12}$, $SrMn_7O_{12}$, and $SrMn_{6.5}Fe_{0.5}O_{12}$ we get "electric polarization" values of 600−1500 $\mu C/m^2$ in $CdMn_7O_{12}$, 220−400 $\mu C/m^2$ in $SrMn_7O_{12}$, and 850 $\mu C/m^2$ in $SrMn_{6.5}Fe_{0.5}O_{12}$ (Figures S25 and S36). As mentioned above, cubic $SrMn_{6.5}Fe_{0.5}O_{12}$ should not be ferroelectric because of its spin-glass magnetic properties. The absence of sharp dielectric anomalies in $CdMn_7O_{12}$ (at 0 Oe), $SrMn_7O_{12}$ (at 0 and 90 kOe), and $SrMn_{6.5}Fe_{0.5}O_{12}$ (at 0 and 90 kOe) is in agreement with our conclusion that the measured electric current is extrinsic. We can rule out a possibility that intrinsic pyrocurrent is overlapped and hidden by significant extrinsic effects because (i) large polarization (with resultant pyrocurrent comparable with the measured TSC current) is expected in $CdMn_7O_{12}$ and $SrMn_7O_{12}$ by analogy with $CaMn_7O_{12}$ and from first-principle calculations,[25] (ii) we found weak but sharp dielectric anomalies and sharp pyrocurrent at T_{N2} in $PbMn_7O_{12}$ even with small intrinsic pyrocurrent overlapping with similar TSC current, and (iii) intrinsic pyrocurrent overlapping with significant TSC current was observed in other multiferroics.[38] Therefore, theoretical predictions of ref 25 for $SrMn_7O_{12}$ about its large polarization have not been confirmed by our results. However, we should mention that no dielectric anomalies were found at T_{N1} and T_{N2} in $CaMn_7O_{12}$ (Figure S12)[21,26,29,37] despite the reported large polarization values (obtained by pyroelectric current measurements in all cases), and in improper ferroelectrics, weak dielectric anomalies are often observed even with large polarization values (e.g., 3*R*-$AgFeO_2$),[43] or no dielectric peaks are detected with small polarization values (e.g., 2*H*-$AgFeO_2$).[44] For further understanding the pyrocurrent and TSC phenomena, systematic investigations of semiconductive properties of AMn_7O_{12} are necessary. And for further understanding the differences among AMn_7O_{12} perovskites with A = Cd, Ca, Sr, and Pb, information about magnetic structures of all members is needed.

5. CONCLUSION

In conclusion, we prepared $CdMn_7O_{12}$ and $SrMn_{7-x}Fe_xO_{12}$ (x = 0, 0.08, and 0.5) perovskites under high pressure (6 GPa) and high temperature (1373−1573 K) conditions, investigated their detailed structural properties above room temperature by synchrotron X-ray powder diffraction, and investigated their detailed magnetic, dielectric, and ferroelectric properties. We found two magnetic transitions in $CdMn_7O_{12}$ with the Néel temperatures T_{N2} = 33 K and T_{N1} = 88 K, and in $SrMn_7O_{12}$ with T_{N2} = 63 K and T_{N1} = 87 K, and structural phase transitions at 493 K in $CdMn_7O_{12}$ and at 404 K in $SrMn_7O_{12}$. We also found differences in magnetic properties, dielectric properties, and hysteresis behavior between $CdMn_7O_{12}$ and $SrMn_7O_{12}$. We discussed general tendencies of the AMn_7O_{12} perovskite family (A = Cd, Ca, Sr, and Pb).

■ ASSOCIATED CONTENT

Supporting Information

The Supporting Information is available free of charge on the ACS Publications website at DOI: 10.1021/acs.inorgchem.5b01472.

Details of structural investigations, magnetic, dielectric, DSC, pyroelectric, and specific heat measurements (PDF)

■ AUTHOR INFORMATION

Corresponding Author

*E-mail: Alexei.Belik@nims.go.jp.

Notes

The authors declare no competing financial interest.

■ ACKNOWLEDGMENTS

This work partially was supported by World Premier International Research Center Initiative (WPI Initiative, MEXT, Japan) and Russian Foundation for Basic Research (RFBR No. 14-03-00768). The synchrotron radiation experiments were performed at the SPring-8 with the approval of the Japan Synchrotron Radiation Research Institute (Proposal Number: 2015A4502).

■ REFERENCES

(1) Vasil'ev, A. N.; Volkova, O. S. *Low Temp. Phys.* **2007**, *33*, 895−914.

DOI: 10.1021/acs.inorgchem.5b01472
Inorg. Chem. 2015, 54, 9081−9091

(2) (a) Shimakawa, Y. *Inorg. Chem.* **2008**, *47*, 8562−8570. (b) Shimakawa, Y.; Mizumaki, M. *J. Phys.: Condens. Matter* **2014**, *26*, 473203.
(3) Yamada, I. *J. Ceram. Soc. Jpn.* **2014**, *122*, 846−851.
(4) Long, Y. W.; Hayashi, N.; Saito, T.; Azuma, M.; Muranaka, S.; Shimakawa, Y. *Nature* **2009**, *458*, 60−63.
(5) Li, J.; Subramanian, M. A.; Rosenfeld, H. D.; Jones, C. Y.; Toby, B. H.; Sleight, A. W. *Chem. Mater.* **2004**, *16*, 5223−5225.
(6) Johnson, R. D.; Chapon, L. C.; Khalyavin, D. D.; Manuel, P.; Radaelli, P. G.; Martin, C. *Phys. Rev. Lett.* **2012**, *108*, 067201.
(7) (a) Ovsyannikov, S. V.; Zainulin, Y. G.; Kadyrova, N. I.; Tyutyunnik, A. P.; Semenova, A. S.; Kasinathan, D.; Tsirlin, A. A.; Miyajima, N.; Karkin, A. E. *Inorg. Chem.* **2013**, *52*, 11703−11710. (b) Shiro, K.; Yamada, I.; Ikeda, N.; Ohgushi, K.; Mizumaki, M.; Takahashi, R.; Nishiyama, N.; Inoue, T.; Irifune, T. *Inorg. Chem.* **2013**, *52*, 1604−1609.
(8) Sánchez-Benítez, J.; Kayser, P.; Morales-García, A.; Martínez-Lope, M. J.; Mompeán, F. J.; Xu, J. M.; Jin, Z. M.; Alonso, J. A. *J. Phys. Chem. C* **2014**, *118*, 9652−9658.
(9) Bochu, B.; Chenavas, J.; Joubert, J. C.; Marezio, M. *J. Solid State Chem.* **1974**, *11*, 88−93.
(10) Marezio, M.; Dernier, P. D.; Chenavas, J.; Joubert, J. C. *J. Solid State Chem.* **1973**, *6*, 16−20.
(11) Prodi, A.; Gilioli, E.; Gauzzi, A.; Licci, F.; Marezio, M.; Bolzoni, F.; Huang, Q.; Santoro, A.; Lynn, J. W. *Nat. Mater.* **2004**, *3*, 48−52.
(12) Gilioli, E.; Licci, F.; Calestani, G.; Prodi, A.; Gauzzi, A.; Salviati, G. *Cryst. Res. Technol.* **2005**, *40*, 1072−1075.
(13) Mezzadri, F.; Calicchio, M.; Gilioli, E.; Cabassi, R.; Bolzoni, F.; Calestani, G.; Bissoli, F. *Phys. Rev. B: Condens. Matter Mater. Phys.* **2009**, *79*, 014420.
(14) Prodi, A.; Gilioli, E.; Cabassi, R.; Bolzoni, F.; Licci, F.; Huang, Q.; Lynn, J. W.; Affronte, M.; Gauzzi, A.; Marezio, M. *Phys. Rev. B: Condens. Matter Mater. Phys.* **2009**, *79*, 085105.
(15) Imamura, N.; Karppinen, M.; Motohashi, T.; Fu, D.; Itoh, M.; Yamauchi, H. *J. Am. Chem. Soc.* **2008**, *130*, 14948−14949.
(16) Mezzadri, F.; Calestani, G.; Calicchio, M.; Gilioli, E.; Bolzoni, F.; Cabassi, R.; Marezio, M.; Migliori, A. *Phys. Rev. B: Condens. Matter Mater. Phys.* **2009**, *79*, 100106(R).
(17) Locherer, T.; Dinnebier, R.; Kremer, R. K.; Greenblatt, M.; Jansen, M. *J. Solid State Chem.* **2012**, *190*, 277−284.
(18) Przenioslo, R.; Sosnowska, I.; Zolltek, M.; Hohlwein, D.; Troyanchuk, I. O. *Phys. B* **1997**, *241−243*, 730−732.
(19) Przenioslo, R.; Sosnowska, I.; Suard, E.; Hansen, T. *Appl. Phys. A: Mater. Sci. Process.* **2002**, *74*, s1731−s1733.
(20) Sanchez-Andujar, M.; Yanez-Vilar, S.; Biskup, N.; Castro-Garcia, S.; Mira, J.; Rivas, J.; Senaris-Rodriguez, M. A. *J. Magn. Magn. Mater.* **2009**, *321*, 1739−1742.
(21) Zhang, G.; Dong, S.; Yan, Z.; Guo, Y.; Zhang, Q.; Yunoki, S.; Dagotto, E.; Liu, J.-M. *Phys. Rev. B: Condens. Matter Mater. Phys.* **2011**, *84*, 174413.
(22) Perks, N. J.; Johnson, R. D.; Martin, C.; Chapon, L. C.; Radaelli, P. G. *Nat. Commun.* **2012**, *3*, 1277−1282.
(23) Motin Seikh, Md.; Caignaert, V.; Lebedev, O. I.; Raveau, B. *Solid State Commun.* **2014**, *180*, 52−55.
(24) Cao, K.; Johnson, R. D.; Perks, N.; Giustino, F.; Radaelli, P. G. *Phys. Rev. B: Condens. Matter Mater. Phys.* **2015**, *91*, 064422.
(25) Liu, H. M.; Dong, S.; Du, Z. Z.; Chu, P.; Liu, J.-M. *EPL* **2014**, *108*, 67012.
(26) Kadlec, F.; Goian, V.; Kadlec, C.; Kempa, M.; Vaněk, P.; Taylor, J.; Rols, S.; Prokleška, J.; Orlita, M.; Kamba, S. *Phys. Rev. B: Condens. Matter Mater. Phys.* **2014**, *90*, 054307.
(27) Du, X.; Yuan, R.; Duan, L.; Wang, C.; Hu, Y.; Li, Y. *Phys. Rev. B: Condens. Matter Mater. Phys.* **2014**, *90*, 104414.
(28) Iliev, M. N.; Hadjiev, V. G.; Gospodinov, M. M.; Nikolova, R. P.; Abrashev, M. V. *Phys. Rev. B: Condens. Matter Mater. Phys.* **2014**, *89*, 214302.
(29) Sannigrahi, J.; Chattopadhyay, S.; Dutta, D.; Giri, S.; Majumdar, S. *J. Phys.: Condens. Matter* **2013**, *25*, 246001.
(30) Bochu, B.; Buevoz, J. L.; Chenavas, J.; Collomb, A.; Joubert, J. C.; Marezio, M. *Solid State Commun.* **1980**, *36*, 133−138.
(31) Belik, A. A.; Matsushita, Y.; Katsuya, Y.; Tanaka, M.; Kolodiazhnyi, T.; Isobe, M.; Takayama-Muromachi, E. *Phys. Rev. B: Condens. Matter Mater. Phys.* **2011**, *84*, 094438.
(32) Tanaka, M.; Katsuya, Y.; Yamamoto, A. *Rev. Sci. Instrum.* **2008**, *79*, 075106.
(33) Tanaka, M.; Katsuya, Y.; Matsushita, Y.; Sakata, O. *J. Ceram. Soc. Jpn.* **2013**, *121*, 287−290.
(34) Izumi, F.; Ikeda, T. *Mater. Sci. Forum* **2000**, *321−324*, 198−205.
(35) Matsnev, M. E.; Rusakov, V. S. *AIP Conf. Proc.* **2012**, *1489*, 178−185.
(36) Brese, N. E.; O'Keeffe, M. *Acta Crystallogr., Sect. B: Struct. Sci.* **1991**, *47*, 192−197.
(37) Przenioslo, R.; Sosnowska, I.; Suard, E.; Hewat, A.; Fitch, A. N. *Phys. B* **2004**, *344*, 358−367.
(38) (a) De, C.; Ghara, S.; Sundaresan, A. *Solid State Commun.* **2015**, *205*, 61−65. (b) Ngo, T. N. M.; Adem, U.; Palstra, T. T. M. *Appl. Phys. Lett.* **2015**, *106*, 152904.
(39) Shi, Y.; Guo, Y.; Shirako, Y.; Yi, W.; Wang, X.; Belik, A. A.; Matsushita, Y.; Feng, H. L.; Tsujimoto, Y.; Arai, M.; Wang, N.; Akaogi, M.; Yamaura, K. *J. Am. Chem. Soc.* **2013**, *135*, 16507−16516.
(40) Ovsyannikov, S. V.; Abakumov, A. M.; Tsirlin, A. A.; Schnelle, W.; Egoavil, R.; Verbeeck, J.; Van Tendeloo, G.; Glazyrin, K. V.; Hanfland, M.; Dubrovinsky, L. *Angew. Chem., Int. Ed.* **2013**, *52*, 1494−1498.
(41) Shannon, R. D. *Acta Crystallogr., Sect. A: Cryst. Phys., Diffr., Theor. Gen. Crystallogr.* **1976**, *32*, 751−767.
(42) Presniakov, I. A.; Rusakov, V. S.; Gubaidulina, T. V.; Sobolev, A. V.; Baranov, A. V.; Demazeau, G.; Volkova, O. S.; Cherepanov, V. M.; Goodilin, E. A.; Knot'ko, A. V.; Isobe, M. *Phys. Rev. B: Condens. Matter Mater. Phys.* **2007**, *76*, 214407.
(43) Terada, N.; Khalyavin, D. D.; Manuel, P.; Tsujimoto, Y.; Knight, K.; Radaelli, P. G.; Suzuki, H. S.; Kitazawa, H. *Phys. Rev. Lett.* **2012**, *109*, 097203.
(44) Terada, N.; Khalyavin, D. D.; Manuel, P.; Tsujimoto, Y.; Belik, A. A. *Phys. Rev. B: Condens. Matter Mater. Phys.* **2015**, *91*, 094434.

DOI: 10.1021/acs.inorgchem.5b01472
Inorg. Chem. 2015, 54, 9081−9091